Chemical Science

ROYAL SOCIETY OF CHEMISTRY

EDGE ARTICLE

View Article Online
View Journal | View Issue

Cite this: *Chem. Sci.*, 2020, **11**, 1269

All publication charges for this article have been paid for by the Royal Society of Chemistry

Received 28th June 2019
Accepted 4th December 2019

DOI: 10.1039/c9sc03191j

rsc.li/chemical-science

Interplay between intrinsically disordered proteins inside membraneless protein liquid droplets†

Yongsang Jo and Yongwon Jung *

Intrinsically disordered proteins (IDPs) in cells phase separate to form diverse membraneless organelles, which have condensed liquid droplet-like properties and often contain multiple IDPs. However, how potential interactions between different IDPs affect the dynamic behavior of these protein droplets is largely unknown. Here, we develop a rapid IDP clustering system to generate protein droplets with varied residue compositions and examine diverse interacting IDPs inside droplets. Three different IDP droplets actively recruited other diverse IDPs inside droplets with extremely varied enrichment (inside/outside) degrees (over 100-fold variation) under highly crowded conditions. The recruited IDPs were mostly mobile even inside highly immobile droplets. Among the five tested IDPs, the disordered region of Ddx4 helicase with its unique multiple charged residue blocks was noticeably influenced by droplet mobility. We also discovered that droplets of different IDPs could rapidly fuse to each other. Interestingly, some droplets were heterogeneously fused with segregated subcompartments, and this segregation was enhanced by droplet maturation and was more apparent for specific IDP pairs, in which the polar and charged residue compositions are highly different. The present study not only reports multiple peculiar behaviors of interacting IDP pairs inside droplets but also provides valuable information on generating membraneless organelle models with controllable droplet properties.

Introduction

Biomolecular condensation in cells generates various membraneless organelles, which retain higher concentrations of biomolecules inside than in the surroundings without discrete physical membrane barriers.[1] These condensates mostly exhibit liquid droplet-like properties such as a round appearance and the ability to fuse to each other.[2] In addition, component molecules exhibit dynamic diffusivity inside and undergo continuous exchange with the outside, potentially enabling spatiotemporal control of biological reactions. Diverse membraneless organelles, such as nucleoli, stress granules, and p-bodies, are known as functional cores of cellular processes, such as gene expression, signal transduction, and stress responses.[3] A series of studies suggested that multivalent interactions between repeated small protein motifs drive protein liquid–liquid phase separation (LLPS), which generates compartmentalized protein liquid droplets.[4]

Many intracellular condensates are highly enriched in proteins that contain structurally undefined regions.[2] These so-called intrinsically disordered proteins/regions (IDPs/IDRs) are compositionally biased and typically comprise particular polar, charged, and aromatic amino acids.[5] It is believed that weak multivalent interactions between these biased residues in IDRs (for example, electro-static,[6] cation–pi[7] or pi–pi interactions[8]) drive LLPS to generate protein liquid droplets with IDP scaffolds.[9] Many protein droplets have been generated with a wide range of IDRs by exceeding or altering the critical concentration for protein phase separation. Interestingly, several IDP droplets showed eventual maturation into less dynamic hydrogel structures or even into irreversible solid fibril aggregates.[10,11]

Membraneless organelles normally include multiple IDPs,[12] and thus interactions between different IDRs could be significant factors for the construction and function of these organelles. Several studies indicated that compositionally biased IDRs might have diverse strengths of affinities with each other. For example, phase-separated droplets of fused in sarcoma (FUS) protein were able to recruit many other FUS family proteins[13] as well as several IDR-containing proteins[11] to varying degrees. Highly concentrated FUS hydrogels also absorbed diverse IDRs with different release rates.[14] At present, however, how interactions between diverse IDRs affect liquid droplet behaviors such as mobility or compartmentalization inside droplets is unknown. Here, we develop an IDR clustering-based protein phase separation system and investigate the interactions between diverse IDRs as droplet forming scaffolds and also as recruited clients (Scheme 1). IDRs with representatively varying amino acid compositions, which primarily govern LLPS-driving residue interactions, were prepared. Subsequently, the

Department of Chemistry, KAIST, 291 Daehak-ro, Yuseong-gu, Daejeon 34143, Republic of Korea. E-mail: ywjung@kaist.ac.kr; Fax: +82-42-350-2810; Tel: +82-42-350-2817

† Electronic supplementary information (ESI) available. See DOI: 10.1039/c9sc03191j

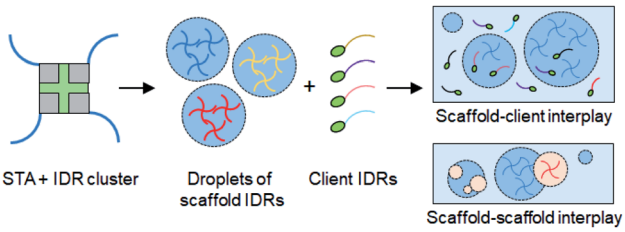

Scheme 1 Schematic of protein liquid droplet formation by rapid clustering of scaffold IDRs by streptavidin (STA). Droplet interactions with other droplets (scaffold–scaffold interplay) and with recruited client IDRs (scaffold–client interplay) are depicted.

mobility and enrichment properties of these interacting IDRs inside droplets were closely examined. Interestingly, IDR affinities to other IDRs as scaffolds were vastly different from those as clients. We also monitored the mixing processes between two IDR droplets. Surprisingly, IDR droplets could rapidly fuse to each other even without commonly binding biomolecules and form multiphase structures.

Results and discussion

Generation of membraneless IDR liquid droplets by protein clustering

Several strategies to generate liquid droplets of IDRs *via* LLPS have been reported. Changes of temperature[15] or salt concentration,[6,11] protein oligomerization,[16,17] and biopolymer (such as RNA) mixing[18–21] are all generally used to trigger IDR phase separation. However, each IDR has different critical concentrations, responses to environmental stimuli, and biopolymer affinities for droplet assembly. To accurately monitor diverse IDR interactions inside and between diverse IDR droplets, the droplet forming conditions must be constant for various IDRs, and components that can interact with IDRs must be minimized. Here we use protein-based rapid clustering of IDRs to generate diverse IDR droplets under the same phase separation conditions. IDR clustering will increase protein multivalency, which is known to enhance the protein LLPS tendency.[2,4] Site-specifically biotinylated IDRs can be rapidly and stably tetramerized by streptavidin (STA),[22] which also has low non-specific interactions with other proteins (Scheme 1). Previously, several optogenetic methods were developed to spatiotemporally induce IDR LLPS in living cells by clustering IDRs with light, where the clustering degree could also be varied.[17,23,24] On the other hand, STA-based clustering provides a fixed valency (4) and is not ideal for cellular applications. Instead, STA offers reliable macroscopic *in vitro* LLPS conditions for diverse IDRs, compared to light-induced cellular protein clustering methods.

We first tested the IDR of fused in sarcoma (FUS) protein, which is known to form IDR protein droplets and recruit several other IDPs into these droplets as discussed above.[11,13] The biotinylated IDR of FUS protein was clustered with STA, and typical spherical liquid droplets[2] were rapidly generated (Fig. 1a and S1†). Dynamic diffusion of the FUS IDR inside the droplets was also confirmed by fluorescence recovery after photobleaching

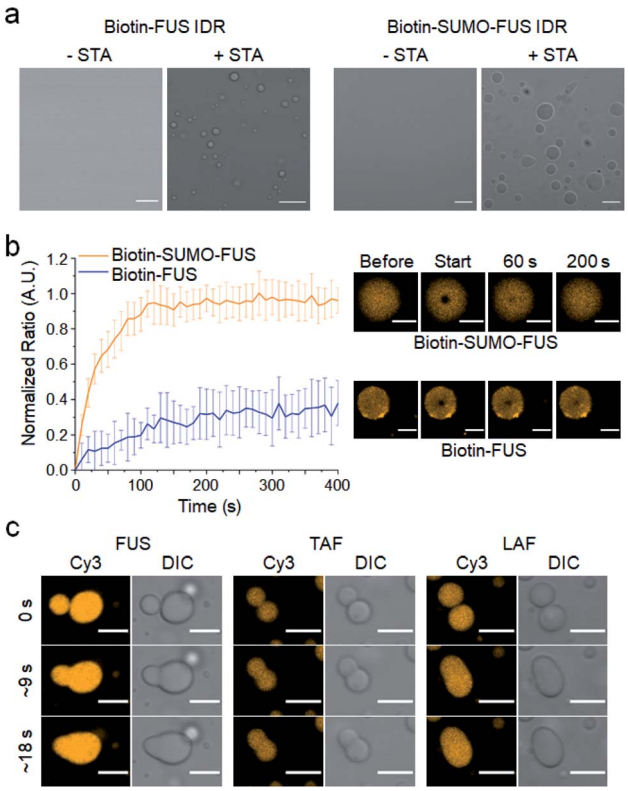

Fig. 1 Formation of IDR protein liquid droplets. (a) Spherical liquid droplet formation by STA-induced clustering of biotinylated FUS IDRs and biotinylated SUMO-fused FUS IDRs. Scale bars: 10 μm. (b) FRAP measurement of dynamic protein diffusion inside FUS droplets at 5 min after phase separation. FRAP recovery curves (left) and images (right) are shown. Error bars: 1 s.d. ($n = 15$ from three independent experiments). Scale bars: 5 μm. (c) Fluorescence images of dynamic fusion between IDR droplets for three IDR scaffolds. Scale bars: 5 μm.

(FRAP) (Fig. 1b). However, only 40% of FUS IDR clusters were mobile in droplets, which is lower than the mobile fractions of several previously reported FUS protein droplets.[10,11] Moreover, the biotinylated FUS IDR was highly prone to aggregation (data not shown). Most endogenous IDPs contain multiple folded domains in addition to their IDRs (Fig. S2a†).[5] Therefore, we added a small and highly soluble SUMO protein domain to the biotin-FUS IDR (biotin-SUMO-FUS IDR). The resulting SUMO-FUS IDR was highly soluble, and STA-induced clustering again rapidly generated SUMO-FUS IDR droplets (Fig. 1a). More importantly, the biotin-SUMO-FUS IDR was mostly mobile inside the droplets, showing properties of more natural FUS droplets.

We also selected two other droplet-forming IDRs (TAF and LAF), which feature amino acid compositions distinct from that of FUS. The IDR of TBP-associated factor 15 (ref. 25) (TAF), which belongs to the FET protein family along with FUS, has more charged residues than that of FUS. On the other hand, the IDR of LAF-1 (ref. 26) protein (LAF) has a significantly lower number of aromatic and polar residues than the FUS and TAF IDRs (protein sequences in the ESI†). Weak interactions between biased IDR residues primarily drive phase separation,

and these residues might also govern IDR droplet properties such as interactions with other IDR proteins. TAF and LAF IDRs were similarly prepared as droplet scaffolds (Fig. S2b†). Upon mixing with STA, these IDRs in the biotin-SUMO cassette also readily formed spherical protein liquid droplets. In addition, all the IDR droplets showed dynamic and rapid fusion between droplets, a representative liquid droplet property (Fig. 1c). The phase separation tendency of each IDR was clearly different, where LAF generated droplets at the lowest concentrations and TAF requires the highest concentrations (Fig. S3†). Addition of a high concentration of crowding reagent (15% PEG), however, allowed us to generate all the IDR droplets under the same conditions and, therefore, it would be possible to reliably investigate diverse IDR interactions with minimized external effects, particularly for different IDR droplets with widely varied residue compositions.

Active recruitment of IDR clients inside IDR droplets

To assess IDR interactions inside droplets, we examined the ability of the three IDR droplets (scaffold) to recruit various other IDRs (client). In addition to the three scaffold IDRs, two more IDRs from well-known constituents of membraneless organelles (again with distinct residue compositions) were also prepared as client IDRs (Fig. S4†). The IDR of Ddx4 helicase[6] (DDX) contains even more charged residues (nearly 30%) than that of LAF (Fig. 2a). The IDR of TIA1 (ref. 27) (TIA) has only a few charged residues similar to that of FUS but is much shorter than the other IDRs. EGFP-fused IDR clients were added to pre-formed IDR droplets. The final protein concentrations of scaffolds and clients were set to 80 : 1 (scaffold : client). The quantitative recruitment propensity was obtained by measuring partition coefficients (PCs), which are ratios of fluorescence mean intensities inside and outside the droplets. First, condensation of droplet-forming scaffold IDRs themselves by droplet formation was quantitated with chemical dye-labeled scaffolds (Cy3-scaffold). Upon droplet formation, scaffold IDRs were highly condensed (enriched) inside with PCs ranging from 20 to 40 (Fig. 2b, c, and S5†).

When client IDRs were treated with these scaffold-condensed droplets, nearly all the client IDRs were clearly recruited to all three droplets, while free EGFP was barely recruited (Fig. 2b). Recruitment degrees significantly varied depending on the scaffold and client IDRs (Fig. 2c and Table S1†) under 15% PEG conditions. FUS, TAF, and TIA clients were moderately localized (enriched) into droplets (PCs 2–20) with FUS showing the weakest recruitment. The PC of monomeric and EGFP-fused FUS (3.9) inside FUS droplets was significantly lower than the STA-clustered FUS scaffold PC (23.2). Notably, EGFP-FUS and EGFP-TIA (both IDRs with only a few charged residues) were hardly localized into highly charged and less polar LAF droplets (PCs 1.2 and 2.6, respectively), similar to free EGFP (PC 1.8). Overall, client recruitment degrees inside droplets showed no correlation with scaffold enrichment degrees. Interestingly, the DDX and LAF clients showed extremely high PCs (100–250), which were even ~five-fold higher than scaffold enrichment PCs. It is not clear how DDX and LAF (both with a high number of charged residues but fewer polar residues) display unprecedentedly strong localization in all IDR droplets. DDX and LAF interactions might be more effective inside droplets than outside, showing even stronger client enrichment than scaffold enrichment. To examine the importance of charged residues in the client to high droplet enrichment, we prepared charge residue-removed LAF (LAF-CR), in which most of the charge residues were mutated to polar residues (Fig. S6†). The resulting LAF-CR residue composition was similar to the FUS residue composition. Interestingly, charge-removed LAF showed dramatically reduced localization in all IDR droplets (PCs 2.5–3.5), even comparable to that of the FUS client. It is also noteworthy that droplet–client recruitment cannot be

a

	Length (a.a.)	Polar (S, T, N, Q)	+ Charge (R, K)	- Charge (D, E)	Aromatic (F, Y, W)	S, Q	G
FUS	213	52.1%	0.5%	2.3%	12.7%	44.1%	24.9%
TAF	208	43.3%	5.8%	11.1%	13.0%	36.1%	19.2%
LAF	168	22.0%	14.3%	11.9%	7.1%	8.3%	35.1%
DDX	236	26.7%	13.6%	15.3%	9.3%	14.8%	18.6%
TIA	96	37.5%	1.0%	1.0%	15.6%	26.0%	15.6%

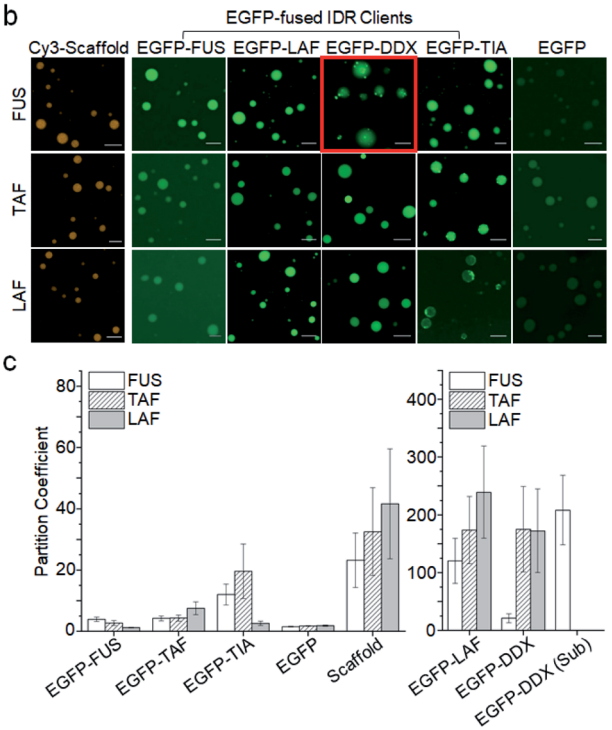

Fig. 2 Recruitment of client IDRs into IDR droplets. (a) Amino acid compositions of IDRs. Polar charged, aromatic, and IDR abundant (S, Q, and G) residues are summarized. (b) Representative fluorescence images of three IDR droplets (FUS, TAF, and LAF) with various EGFP-fused client IDRs and free EGFP (green). Cy3-tagged scaffold IDRs (orange) were used to measure scaffold IDR enrichment inside droplets. The image of EGFP-DDX subcompartments in FUS droplets is indicated with a red box. Scale bars: 10 μm. (c) Partition coefficients (PCs) (inside/outside droplets) of client EGFP-IDRs, free EGFP, and Cy3-scaffolds. The PC of EGFP-DDX sub-compartments inside FUS droplets (EGFP-DDX (Sub)) is also shown. Error bars: 1 s.d. (n = 100 from three independent experiments).

simply explained with affinities between IDR pairs. For example, FUS droplets can strongly recruit LAF, but LAF droplets do not recruit FUS. We also examined whether this paradoxical observation is still valid in the absence of protein clustering or under more physiologically crowded conditions. The recruitment tendency of the LAF and FUS clients was consistent even without STA clustering or with less PEG (physiologically relevant 1.5% PEG[28] or 0% PEG rather than 15% PEG) (Fig. S7†). Overall client enrichments inside droplets were, however, dramatically reduced with lowered PEG concentrations.

We also observed that the recruited DDX client formed unique subcompartments inside the FUS droplets (red box in Fig. 2b). Recruited DDX was further enriched (~10-fold) in these subcompartments (Fig. 2c), which were also distinguishable from the FUS droplets in the contrast images (Fig. S8†). This unique behavior of DDX inside FUS droplets could be caused by its amino acid composition. The abundant charged residues of DDX form characteristic multiple charged peptide blocks, which provide stronger protein interactions than scattered charged residues,[6] possibly leading to DDX condensation inside the FUS droplets. In fact, when charged residues of DDX were randomly scrambled,[6] DDX subcompartments inside FUS droplets were not observed at all (Fig. S9†).

We next examined oligonucleotide (ON) recruitment since many membraneless organelles also contain nucleic acids. Only LAF droplets visibly recruited ONs (PCs: 6.5 for RNA, 1.9 for single-stranded DNA, and 1.2 for double-stranded DNA), while FUS and TAF droplets even slightly excluded ONs (Fig. S10†). ON recruitment is likely driven by the abundant positive residues in LAF droplets (Fig. 2a), even without any specific ON binding motifs. Control of DNA recruitment into droplets and exclusion from droplets was also possible by mixing varying ratios of two IDR scaffolds (Fig. S11†), which can be a potential strategy for selective biomolecular compartmentalization.

The PCs of scaffolds were not altered by client addition (proteins and ONs) (Fig. S12†), indicating that the scaffold condensation processes are mostly unaffected by small portions of clients. When droplets were generated by IDR dimerization rather than tetramerization, the recruitment tendency was similar for all the clients, but the overall PCs including scaffold enrichment were lowered (Fig. S13†). The data suggest that enhanced clustering of scaffold IDRs facilitates enhanced scaffold condensation as well as enhanced client recruitment.

Dynamic diffusion of interacting IDRs inside droplets

We next investigated the relative mobility of the scaffold and client IDRs inside droplets. Since maturation of several IDR droplets into less-mobile structures has been reported,[11,13] scaffold diffusion was examined at 1 h after droplet formation. While FUS and LAF droplets were mostly mobile, only 40% of the TAF scaffold was mobile (Fig. 3a). On the other hand, most client IDRs including ONs are highly mobile inside all the droplets including heavily matured TAF droplets (Fig. 3b and S14, Table S2†). Client IDRs might have characteristic high mobility (generally mobile) inside droplets regardless of

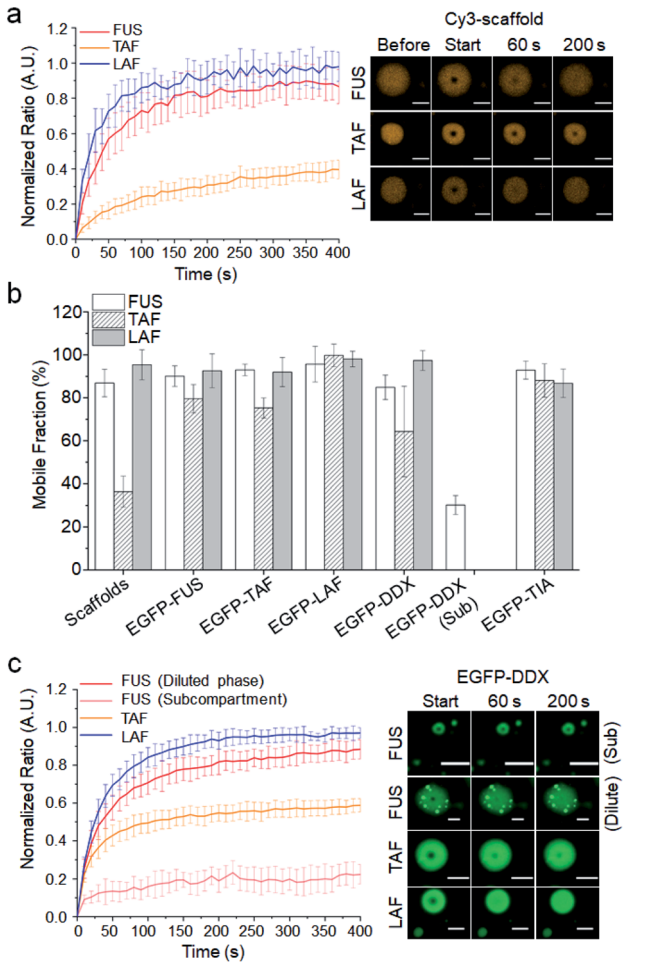

Fig. 3 Dynamic diffusion of scaffold and client IDRs inside droplets. (a) FRAP recovery curves and images of three scaffold IDRs after 1 h of maturation. (b) Mobile fractions of scaffold and client IDRs inside the three IDR droplets (including DDX subcompartments) after 1 h of maturation. (c) FRAP recovery curves and images of client EGFP-DDX in IDR droplets including FUS droplets with EGFP-DDX subcompartments (Sub). Error bars: 1 s.d. ($n = 15$ from three independent experiments). Scale bars: 5 μm.

scaffold mobility or affinity, although EGFP fusion could also affect client mobility. For example, the client LAF, which showed strong recruitment (affinity) to TAF droplets (Fig. 2), was still highly mobile inside the largely immobile TAF droplets.

Only the client DDX displayed a somewhat scaffold-dependent mobility decrease (Fig. 3c). While EGFP-DDX was highly mobile in the mobile LAF droplets, its mobile fraction was significantly decreased in the immobile TAF droplets. In addition, subcompartments of EGFP-DDX in the FUS droplets were also highly immobile, while EGFP-DDX in the diluted parts of droplets was mobile. We further tested scaffold maturation over 2 h. TAF droplets showed the fastest decrease of the mobile fraction (30% after 2 h), and FUS droplets also showed moderate maturation (~70% mobile after 2 h), while LAF droplets were highly mobile even after 2 h (Fig. S15†). Again, only the client DDX clearly showed a mobility decrease inside the TAF droplets as TAF

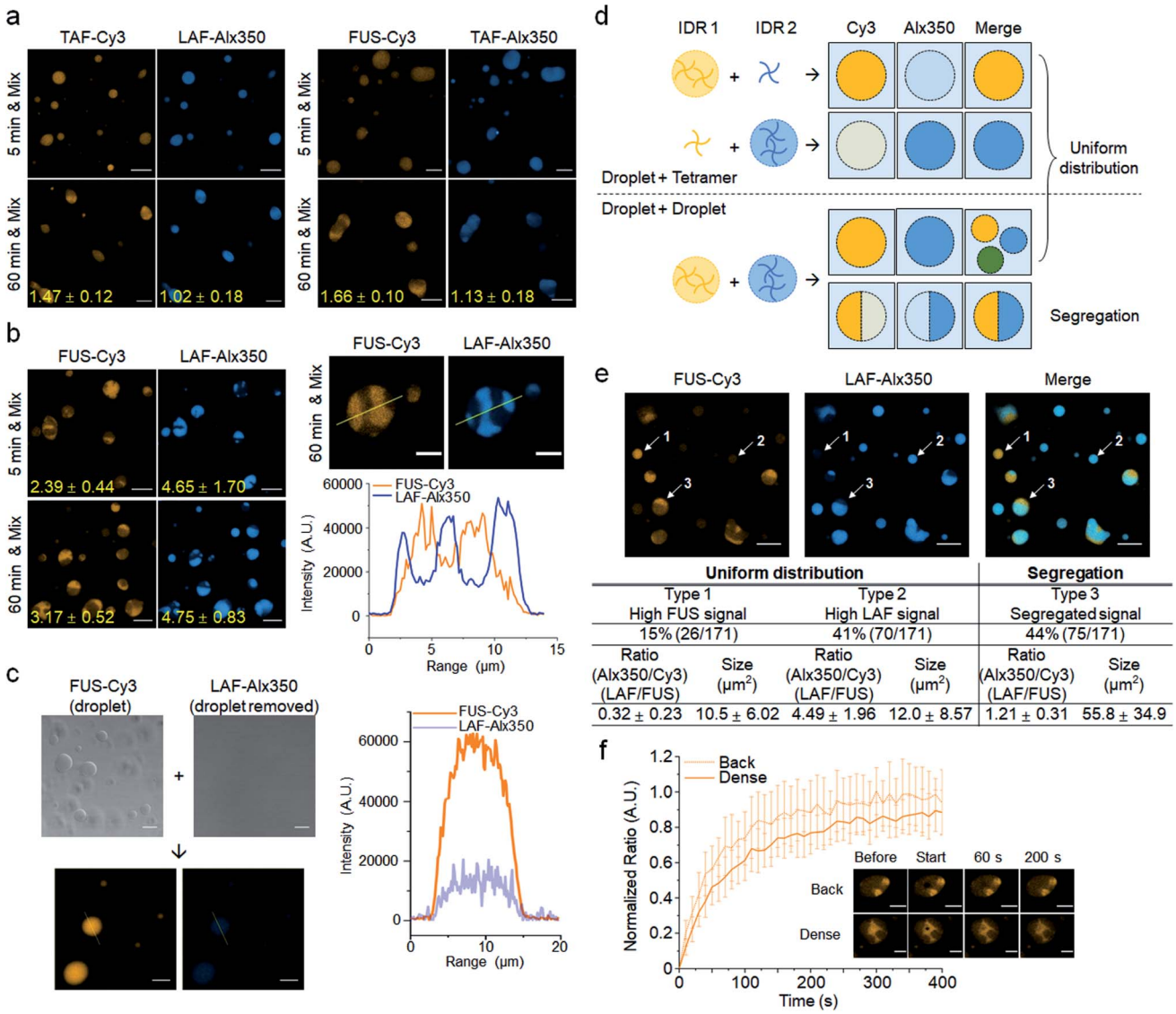

Fig. 4 Dynamic fusion between different droplets after maturation. (a) Fluorescence images of two differently labeled mixed IDR droplets. TAF droplets were mixed with LAF (left) or FUS (right) droplets after 5 min or 1 h maturation and incubated for 5 min. Ratios of fluorescence mean intensities of the dense and diluted phases of segregated droplets are indicated with yellow numbers. Scale bars: 10 μm. (b) Fusion between LAF and FUS droplets. Fluorescence images and intensity profiles of LAF/FUS fused multiphase droplets are shown (right). The fluorescence profiles are obtained using the yellow lines that cross through multiphase droplets. Scale bars: 10 μm (left) and 5 μm (right). (c) Fusion between FUS droplets and the droplet-removed free LAF tetramer. Contrast images of FUS droplets and LAF tetramers before mixing are also shown. Scale bars: 10 μm. (d) Schematic diagram of the mixing processes between two differently labeled IDR droplet solutions. Possible fluorescence images for Cy3 (yellow) and Alx350 (blue) dyes and merged images are depicted. (e) Analysis of a FUS and LAF droplet mixture. Droplets were matured for 1 h before mixing. Representative droplets of uniformly distributed droplets with high FUS (type 1) or high LAF (type 2) and segregated droplets (type 3) are indicated with arrows and numbers. Population, relative IDR ratios, and sizes of these three types of droplets are summarized below (n = 171 from 5 independent experiments). Scale bars: 10 μm. (f) FRAP recovery curves and images of the dense and diluted phases of LAF/FUS fused droplets. Error bars: 1 s.d. (n = 15 from three independent experiments). Scale bars: 5 μm.

scaffolds matured and became less mobile over time (Fig. S16†). Diffusion of other client IDRs was not affected by scaffold maturation. It is not clear why only client DDX showed scaffold-dependent mobility changes. Indeed, LAF and DDX both have abundant charged residues unlike the other IDRs and also showed high enrichment in IDR droplets as clients (Fig. 2). One clear difference between DDX and LAF is its unique charged residue blocks. Interestingly, charge-scrambled DDX showed increased mobility inside matured TAF droplets (Fig. S17†). Inside 2 h-matured TAF droplets, the mobile fraction of charge-scrambled DDX was 65%, while that of wild-type DDX was only 44%. The data suggest that charged blocks of DDX may contribute to the unique diffusion behavior of DDX inside IDR droplets. There are also residue differences in the Ser, Gln and Gly contents (LAF: S, Q 8.3% and G 35.1%; DDX: S, Q 14.8% and G 18.6%). Previously, Wang and colleagues showed that Ser and Gln are 'droplet-hardening' residues, which can reduce the mobile fractions of FUS IDP droplets, while Gly is a 'droplet-softening' residue, which

shows an opposite effect.[12] DDX with more Ser and Gln and less Gly residues might be more sticky than LAF inside droplets and influenced more by the surrounding scaffold IDRs.

Dynamic interactions between different IDR droplets

There are many examples of multiphase (such as core–shell) cellular droplets, where segregated parts exist inside droplets with each compartment enriched by different proteins.[2,29,30] A recent study demonstrated that two different immiscible IDR droplets with different surface tensions can form multiphase droplets by adding commonly binding (to both droplets) RNA.[29] Without any commonly binding entities, we investigated interactions between the three IDR droplets, which showed varying IDR affinities to each other (droplet enrichment propensity: FUS < TAF < LAF) and also different maturation traits (maturation propensity to less-mobile structures: LAF < FUS < TAF). TAF droplets, which showed the fastest maturation, were first mixed with FUS or LAF droplets at 5 min or 1 h after phase separation. Two different droplets that were labeled with different dyes were incubated for 5 min before fluorescence imaging analysis. Even only after 5 min of incubation, all the droplets showed fluorescence signals of both mixed IDRs (Fig. 4a). However, while TAF and LAF (or FUS) were uniformly distributed (miscible) in mixed droplets with 5 min of maturation, weak but clear phase segregation was observed with 1 h of maturation (Fig. 4a and S18†). Ratios of the fluorescence mean intensities of the dense and diluted phases exceeded 1.6 for FUS droplets with TAF scaffolds, indicating that maturation of droplets could reduce their miscibility. On the other hand, when we mixed FUS and LAF droplets, the mixed droplets showed strong phase segregation even with only 5 min of maturation (Fig. 4b). Signal ratios of dense and diluted phases easily exceeded 4 for LAF scaffolds inside FUS + LAF droplets. These subcompartments also showed liquid-like fusion inside droplets (Fig. S19†).

During mixing of two IDR droplet solutions, droplets with both IDR signals can be generated *via* multiple routes. Since a portion of STA-clustered IDR tetramers can exist freely outside the droplets, these free IDR tetramers can be recruited to other IDR droplets as clients. On the other hand, two different droplets can also directly fuse to each other to form even larger droplets. In fact, many large droplets were observed in the droplet mixtures (Fig. 4a and b). To elucidate this droplet mixing process, we prepared a free LAF tetramer solution without LAF droplets by removing the droplets by centrifugation after LLPS. When this clear, droplet-removed LAF tetramer solution was mixed with FUS droplets, we only observed droplets with uniformly distributed FUS (strong) and LAF (weak) signals (LAF/FUS: 0.28 ± 0.02) without any segregation (Fig. 4c). The data strongly support that segregated multiphase LAF–FUS droplets are generated by direct droplet–droplet fusion. Upon droplet mixing, there will be droplets with recruited IDR tetramers, which would have a rather uneven population of the two IDRs (lower signals for clients) and also droplets generated by droplet–droplet fusion, which can have segregated forms (Fig. 4d). When we analyzed the mixture of 1 h matured FUS and LAF droplets, 44% of droplets exhibited clear segregation (Fig. 4e). In fact, these segregated droplets are generally bigger ($\sim$55 μm^2) than uniformly distributed droplets (10–12 μm^2), supporting the finding that segregated droplets were generated by droplet fusion. In addition, LAF/FUS ratios (Alx350/Cy3) inside segregated droplets are relatively even (1.21), while the other 56% of smaller droplets without segregation have clearly uneven IDR ratios (Alx350/Cy3: 0.32 or 4.49). Among these small droplets, It is likely that 15% of droplets mostly represent FUS droplets with LAF tetramers (type 1, LAF/FUS: 0.32; also see Fig. 4c) and the other 41% of droplets are LAF droplets with FUS tetramers (type 2, LAF/FUS: 4.49). Similarly, when FUS and TAF or TAF and LAF droplets (with 1 h of maturation) were mixed, larger droplets with similar signals of the two IDRs showed segregated multiphases (Fig. S20†). However, since droplet segregation was weaker in the FUS + TAF and TAF + LAF mixtures (Fig. 4a), segregated droplets were clearly less abundant ($\sim$23%). Taking these results together, this is the first observation that droplets of interacting IDR scaffolds can rapidly fuse and sometimes form multiphase droplets depending on maturation. It is possible that strong phase segregation of FUS + LAF droplets is due to large polar and charged residue differences between FUS and LAF (Fig. 2a). As previously reported, IDR droplets with different surface tensions can form multiphase droplets.[29] We also measured the surface tensions of FUS, TAF, and LAF droplets. Both the FUS and LAF droplets showed high surface tensions, while the TAF droplets showed the lowest surface tension (Fig. S21†). Since the FUS + LAF droplets showed the strongest phase segregation (Fig. 4), IDR droplet properties other than surface tension can also likely contribute to the formation of the segregated IDR phases.

Scaffold FUS and LAF IDRs in the dense or diluted phase of multiphase droplets were as mobile as single-phase droplets (Fig. 4f and S22†). Dense phases of TAF were also largely immobile similar to the TAF-only droplets with 1 h of maturation. On the other hand, TAF in the diluted phase was highly mobile, indicating that diffusivity can be varied by subcompartment formation inside droplets. When the initial droplets were generated with two IDRs and incubated for maturation, multiphase separation was largely diminished (Fig. S23†). Only FUS + LAF droplets with 1 h of maturation displayed weak multiphase separation. Maturation before droplet fusion (not after fusion) can effectively enhance multiphase segregation. In addition, multiphase separation was also weakened when droplets were generated without IDR clustering (Fig. S24†). Enhanced LLPS by IDR clustering is also important for the observed multiphases of fused droplets.

Conclusions

We developed a protein clustering cassette to investigate the behaviors of diverse interacting IDRs inside and between membraneless organelle models. Nearly all the tested IDRs with extensively varied residue compositions were recruited to droplets, while the enrichment degrees were highly varied (PCs ranging from 2 to over 200), and some clients even showed higher enrichment than the scaffolds under highly crowded conditions. Also, the FUS and LAF IDRs paradoxically recruited each other (FUS droplets recruit LAF, but not *vice versa*) regardless of

molecular crowding or clustering. Most recruited IDRs were highly mobile inside the droplets, largely independent of scaffold mobility. We also observed that different IDR droplets rapidly fuse to each other without commonly binding biomolecules, and they can form multiphase droplets with a clear dependency on droplet maturation and IDR residue compositions. While we showed how IDRs with their distinct residue compositions display uniquely different behaviors as scaffolds and clients, further studies must focus on the detailed molecular codes of IDRs, which determine these vastly varied IDR behaviors. The present discovery can also be used to generate various membraneless organelle models, where client enrichment, droplet mobility, and subcompartment formation can be tunable by selecting the appropriate IDRs. We expect that diverse biochemical processes in various biomolecular condensate environments can be monitored with these versatile droplet models.

Conflicts of interest

There are no conflicts to declare.

Acknowledgements

This work is supported by the Samsung Science & Technology Foundation (SSTF-BA1501-09).

Notes and references

1 S. Boeynaems, S. Alberti, N. L. Fawzi, T. Mittag, M. Polymenidou, F. Rousseau, J. Schymkowitz, J. Shorter, B. Wolozin, L. Van Den Bosch, P. Tompa and M. Fuxreiter, *Trends Cell Biol.*, 2018, **28**, 420–435.
2 Y. Shin and C. P. Brangwynne, *Science*, 2017, **357**, eaaf4382.
3 D. S. W. Protter and R. Parker, *Trends Cell Biol.*, 2016, **26**, 668–679.
4 S. F. Banani, H. O. Lee, A. A. Hyman and M. K. Rosen, *Nat. Rev. Mol. Cell Biol.*, 2017, **18**, 285–298.
5 H. J. Dyson and P. E. Wright, *Nat. Rev. Mol. Cell Biol.*, 2005, **6**, 197–208.
6 T. J. Nott, E. Petsalaki, P. Farber, D. Jervis, E. Fussner, A. Plochowietz, T. D. Craggs, D. P. Bazett-Jones, T. Pawson, J. D. Forman-Kay and A. J. Baldwin, *Mol. Cell*, 2015, **57**, 936–947.
7 S. Qamar, G. Wang, S. J. Randle, F. S. Ruggeri, J. A. Varela, J. Q. Lin, E. C. Phillips, A. Miyashita, D. Williams, F. Strohl, W. Meadows, R. Ferry, V. J. Dardov, G. G. Tartaglia, L. A. Farrer, G. S. Kaminski Schierle, C. F. Kaminski, C. E. Holt, P. E. Fraser, G. Schmitt-Ulms, D. Klenerman, T. Knowles, M. Vendruscolo and P. St George-Hyslop, *Cell*, 2018, **173**, 720–734.
8 R. M. Vernon, P. A. Chong, B. Tsang, T. H. Kim, A. Bah, P. Farber, H. Lin and J. D. Forman-Kay, *eLife*, 2018, **7**, e31486.
9 C. W. Pak, M. Kosno, A. S. Holehouse, S. B. Padrick, A. Mittal, R. Ali, A. A. Yunus, D. R. Liu, R. V. Pappu and M. K. Rosen, *Mol. Cell*, 2016, **63**, 72–85.
10 A. Patel, H. O. Lee, L. Jawerth, S. Maharana, M. Jahnel, M. Y. Hein, S. Stoynov, J. Mahamid, S. Saha, T. M. Franzmann, A. Pozniakovski, I. Poser, N. Maghelli, L. A. Royer, M. Weigert, E. W. Myers, S. Grill, D. Drechsel, A. A. Hyman and S. Alberti, *Cell*, 2015, **162**, 1066–1077.
11 Y. Lin, D. S. Protter, M. K. Rosen and R. Parker, *Mol. Cell*, 2015, **60**, 208–219.
12 V. N. Uversky, *Curr. Opin. Struct. Biol.*, 2017, **44**, 18–30.
13 J. Wang, J. M. Choi, A. S. Holehouse, H. O. Lee, X. Zhang, M. Jahnel, S. Maharana, R. Lemaitre, A. Pozniakovsky, D. Drechsel, I. Poser, R. V. Pappu, S. Alberti and A. A. Hyman, *Cell*, 2018, **174**, 688–699.
14 M. Kato, T. W. Han, S. Xie, K. Shi, X. Du, L. C. Wu, H. Mirzaei, E. J. Goldsmith, J. Longgood, J. Pei, N. V. Grishin, D. E. Frantz, J. W. Schneider, S. Chen, L. Li, M. R. Sawaya, D. Eisenberg, R. Tycko and S. L. McKnight, *Cell*, 2012, **149**, 753–767.
15 A. Molliex, J. Temirov, J. Lee, M. Coughlin, A. P. Kanagaraj, H. J. Kim, T. Mittag and J. P. Taylor, *Cell*, 2015, **163**, 123–133.
16 B. S. Schuster, E. H. Reed, R. Parthasarathy, C. N. Jahnke, R. M. Caldwell, J. G. Bermudez, H. Ramage, M. C. Good and D. A. Hammer, *Nat. Commun.*, 2018, **9**, 2985.
17 Y. Shin, J. Berry, N. Pannucci, M. P. Haataja, J. E. Toettcher and C. P. Brangwynne, *Cell*, 2017, **168**, 159–171.
18 S. Maharana, J. Wang, D. K. Papadopoulos, D. Richter, A. Pozniakovsky, I. Poser, M. Bickle, S. Rizk, J. Guillen-Boixet, T. M. Franzmann, M. Jahnel, L. Marrone, Y. T. Chang, J. Sterneckert, P. Tomancak, A. A. Hyman and S. Alberti, *Science*, 2018, **360**, 918–921.
19 H. Zhang, S. Elbaum-Garfinkle, E. M. Langdon, N. Taylor, P. Occhipinti, A. A. Bridges, C. P. Brangwynne and A. S. Gladfelter, *Mol. Cell*, 2015, **60**, 220–230.
20 P. R. Banerjee, A. N. Milin, M. M. Moosa, P. L. Onuchic and A. A. Deniz, *Angew. Chem., Int. Ed.*, 2017, **56**, 11354–11359.
21 W. M. Aumiller Jr and C. D. Keating, *Nat. Chem.*, 2016, **8**, 129–137.
22 C. M. Dundas, D. Demonte and S. Park, *Appl. Microbiol. Biotechnol.*, 2013, **97**, 9343–9353.
23 D. Bracha, M. T. Walls, M. T. Wei, L. Zhu, M. Kurian, J. L. Avalos, J. E. Toettcher and C. P. Brangwynne, *Cell*, 2018, **175**, 1467–1480.
24 P. Zhang, B. Fan, P. Yang, J. Temirov, J. Messing, H. J. Kim and J. P. Taylor, *eLife*, 2019, **8**, e39578.
25 M. Altmeyer, K. J. Neelsen, F. Teloni, I. Pozdnyakova, S. Pellegrino, M. Grofte, M. B. Rask, W. Streicher, S. Jungmichel, M. L. Nielsen and J. Lukas, *Nat. Commun.*, 2015, **6**, 8088.
26 S. Elbaum-Garfinkle, Y. Kim, K. Szczepaniak, C. C. Chen, C. R. Eckmann, S. Myong and C. P. Brangwynne, *Proc. Natl. Acad. Sci. U. S. A.*, 2015, **112**, 7189–7194.
27 N. Gilks, N. Kedersha, M. Ayodele, L. Shen, G. Stoecklin, L. M. Dember and P. Anderson, *Mol. Biol. Cell*, 2004, **15**, 5383–5398.
28 T. J. Mitchison, *Mol. Biol. Cell*, 2019, **30**, 173–180.
29 M. Feric, N. Vaidya, T. S. Harmon, D. M. Mitrea, L. Zhu, T. M. Richardson, R. W. Kriwacki, R. V. Pappu and C. P. Brangwynne, *Cell*, 2016, **165**, 1686–1697.
30 S. Jain, J. R. Wheeler, R. W. Walters, A. Agrawal, A. Barsic and R. Parker, *Cell*, 2016, **164**, 487–498.